



# Influence of the reinforcement on penetration and perforation of concrete targets

Penetration and perforation

## A discrete element analysis

29

Wenjie Shiu, Frédéric Victor Donzé and Laurent Daudeville  
*Soils Solids Structures Laboratory, Joseph Fourier University,  
 Grenoble, France*

### Abstract

**Purpose** – The purpose of this paper is to describe how a discrete element model is used to predict the penetration depth and the perforation caused by a non-deformable missile against a thin reinforced concrete slab.

**Design/methodology/approach** – Initial calibration of the model was done with a series of flat-nose missile tests. Additional simulations were performed with varying the percentage of reinforcement. The present numerical model is compared to experimental test data provided by the French Atomic Energy Agency (CEA) and the French Electrical Power Company (EDF).

**Findings** – For thin concrete slabs, the evolution of the penetration depth in terms of percentage of reinforcement was compared with experimental results: quantitatively the results are very coherent.

**Originality/value** – The modeling scale is higher than the heterogeneity scale, so the model may be used to simulate real structures, which means that the discrete element method is mainly used here for its ability to account for discontinuities; an identification process based on quasi-static tests is used, so the quasi-static behavior of concrete is reproduced. This identification process is the key point, to allow a complete predictive computation for complex impact configurations, especially when the missile diameter and the thickness of the concrete slab are on the same order in size.

**Keywords** Concrete slabs, Reinforced concrete, Modelling, Impact strength

**Paper type** Research paper

### Nomenclature

$A_{(i)}$	= the generalized acceleration	$J$	= the polar moment of the disk's cross-section (between two bonding elements)
$D$	= the diameter of the missile	$K_i$	= the $i$ -th component of the element stiffness
$d_p$	= the slab thickness	$kn$	= the normal stiffness of the element
$E_c$	= Young's modulus of the concrete	$\bar{k}^n$	= (also noted $Pb\_kn$ ) the normal stiffness of the parallel bond
$E_s$	= Young's modulus of the steel reinforcement	$ks$	= the tangent stiffness of the element
$F_i$	= the $i$ -th component of the generalized contact force	$\bar{k}^s$	= (also noted $Pb\_ks$ ) the tangent stiffness of the parallel bond
$F_{(i)}^d$	= the damping force		
$f_c$	= the compressive stress of a concrete target		
$g$	= the gravitational acceleration		
$I$	= the moment of inertia		
$I_d$	= the impact function (= $(Mv^2/D^3f_c)/82.6f_c^{-0.544}$ )		



k	= the dimensionless penetration depth	$U_i$	= the overlap between two elements in contact
M	= the mass of the missile	v	= the impact velocity
$M_i$	= the generalized moment acting on each element	$v_p$	= the ballistic limit
$\bar{M}_i^n$	= the normal generalized moment acting on each parallel bond	$X$	= the penetration depth
$\bar{M}_i^s$	= the tangent generalized moment acting on each parallel bond	$\ddot{x}_i$	= the translation acceleration
m	= the mass of the element	<i>Greek symbols</i>	
$N_d$	= the geometry function (= $(M/\rho_c D^3)$ )	$\alpha$	= numerical damping factor
Pb_nstrength	= parallel bond maximum normal stress	$\mu$	= the friction coefficient
Pb_sstrength	= parallel bond maximum shear stress	$\Delta\theta^n$	= the normal relative angular rotation between two elements in contact
r	= the reinforcement ratio	$\Delta\theta^s$	= the tangent relative angular rotation between two elements in contact
		$\omega_i$	= the rotational acceleration
		$\rho_c$	= the density of a concrete target

### 1. Introduction

The design of concrete structures to protect against severe impacts requires models with high-predicting capabilities. These models consider four major quantities (Degen, 1980; Hughes, 1984), which measure the local impact effects on a concrete structure: the penetration depth, the scabbing, the perforation and the ballistic limits. The penetration depth is the distance a projectiles penetrates a thick concrete target without resulting in perforation and scabbing. The perforation or scabbing limit is the minimum thickness of the target to prevent perforation or scabbing and the ballistic limit is the minimum initial impact velocity to perforate the target.

Many of the available protective design guidelines recommend the use of empirical approaches for the assessment of penetration, scabbing and perforation (Li *et al.*, 2006). For instance, the CEA-EDF formula (Berriaud *et al.*, 1978) is a perforation limit criterion based on a series of weight drops and air gun tests to develop reliable predictions on the ballistic performance of reinforced concrete slabs undergoing a missile impact.

The available empirical formulae were mainly developed by data-fitting of test results. Consistent results over the ordnance velocity range were observed for the different approaches and the main differences begin at the lower impact velocities in non-military applications (Williams, 1994). However, some of them are dimensionally non homogenous and thus, unit dependent, which provide little physical meaning of the local impact event (Li and Tong, 2003). In addition, the application range of the formulae depends on the tests performed. Theoretical and analytical approaches, such as numerical studies are also conducted to overcome the shortcomings of these empirical formulae to get a better understanding of the problem.

The discrete element method (DEM) (Cundall and Strack, 1979), which is an alternative numerical method to continuum-type methods, is used here to study the behavior of concrete structures subjected to rigid impacts. This method does not rely upon any assumption about where and how a crack or several cracks occur and propagate, since the medium is naturally discontinuous and is very well adapted to dynamic problems, when a transition from the solid state to a granular flow regime is observed.

Nevertheless, when a DEM model is used, the issue of the modeling scale has to be addressed: the DEM is well adapted to the modeling of granular material, where an element represents a grain (Cundall and Strack, 1979; Iwashita and Oda, 2000). Numerous authors have also used the DEM to simulate cohesive geomaterials such as concrete, at the heterogeneity scale (Potapov *et al.*, 1995; Potyondy *et al.*, 1996), i.e. the size of an element is on the order of the size of the biggest heterogeneity. This approach gives a better understanding of concrete fracture, but makes the modeling of real structures difficult because of the computational cost. Another way to use the DEM consists in using a higher scale model, which considers that the whole collection of elements must reproduce the macroscopic behavior of concrete. Such an approach was mainly developed in 2D (Magnier and Donzé, 1998; Meguro and Hakuno, 1989) or in 3D with a regular assembly of discrete elements (DE) (Riera and Iturrioz, 1998).

In order to get more insight into the perforation process of a concrete slab subjected to rigid flat-nose shaped missile impacts, a real 3D reinforced concrete structure has been simulated with the DEM. In the following work, the prediction of the missile trajectory was compared with experimental data. Before this last step was possible, the model had to go through a validation process through quasi-static uniaxial tests, which allowed the minimum definition of a parameter identification process (Hentz *et al.*, 2003): thus, the modeling scale imposed by the available computing power is controlled, and the simulations are capable of predicting the observed perforation limits.

This 3D approach can predict the penetration depth or the perforation residual velocity of the missile. Moreover, the influence of the reinforcement ratio on the perforation process has been analyzed since the available empirical formulae either neglect this parameter or take it into account in a simplified way.

## 2. The DEM model

Following impact simulations (Magnier and Donzé, 1998; Camborde *et al.*, 2000), in which the SDEC code was used (Donzé and Magnier, 1997), the potentiality of the PFC<sup>3D</sup> code (2003) to simulate real test cases is now investigated.

In the PFC<sup>3D</sup> code, the DE are spherical and interact with a force-displacement type law (equation (1a)). The equations of motion applied to each element are defined by equations (1b) and (1c):

$$F_i = K_i U_i \quad (1a)$$

$$F_i = m(\ddot{x}_i - g_i) \quad (\text{translational motion}) \quad (1b)$$

$$M_i = I\ddot{\omega}_i \quad (\text{rotational motion}) \quad (1c)$$

where  $F_i$  is the  $i$ -th component of the contact force,  $K_i$  the stiffness associated to each element, with  $kn$  in the normal direction and  $ks$  in the tangent direction,  $U_i$  is the overlap between two elements in contact,  $m$  is the mass of each element,  $\ddot{x}$  and  $\ddot{\omega}$  are the translational acceleration and rotational acceleration, respectively,  $g$  is the gravitational acceleration,  $M_i$  is the resultant moment acting on each element and  $I$  is the moment of inertia. During the calculation cycle, the force-displacement law (equation (1a)) is calculated first, then the new element's position will be updated by the law of motion (equations (1b) and (1c)). Note that more information about the formulation of PFC<sup>3D</sup> can be found in PFC<sup>3D</sup> code (2003).

PFC<sup>3D</sup> provides two ways of formulating the interaction between two elements: the contact and parallel bonds. Because the present objective was to simulate concrete which

is a frictional-cohesive material, the parallel bond has been chosen for the numerical modeling since it can transfer both the contact force and moment between two elements in contact. The parallel bond is to be treated as glue lying on a finite circular cross-section between two elements. To form a parallel bond, its stiffness and yield stress should be defined before the calculation as well. Thus, new intrinsic parameters are involved, such as, pb\_kn, pb\_ks, pb\_nstrength, pb\_sstrength which are normal and tangent stiffness, and normal and shear yield stress, respectively. The stress which acts on the parallel bond was calculated via the beam theory (Figure 1). If either of the maximum stresses exceeds its corresponding bond resistance, the parallel bond breaks. Thus, a simple elastic-brittle behavior was used here. The transferring force in a parallel bond is described in equation (2) by replacing the stiffness terms by pb\_kn and pb\_ks. The moment transfers between two bonded elements is calculated by:

$$\bar{M}_i^n = \bar{k}^s J \Delta\theta^n \quad (2a)$$

$$\bar{M}_i^s = \bar{k}^n I \Delta\theta^s \quad (2b)$$

where  $\bar{M}_i^n$  and  $\bar{M}_i^s$  are the normal and tangent generalized moments,  $\bar{k}^n$  and  $\bar{k}^s$  are the normal and the tangent stiffnesses of the parallel bond,  $J$  is the polar moment of the disk's cross-section,  $I$  is the moment of inertia of the disk's cross-section,  $\Delta\theta^n$  and  $\Delta\theta^s$  are the normal and the tangent relative angular rotation between two elements in contact. Furthermore, when a parallel bond exists between two elements, slip may occur between these bonded elements.

Energy dissipation was also used in our numerical model. The energy involved between two interacting elements is dissipated through frictional sliding for which a Coulomb friction coefficient  $\mu$  is defined. Moreover, a local non-viscous damping is available in PFC<sup>3D</sup>, where the damping force is put together with the equation of motion such that:

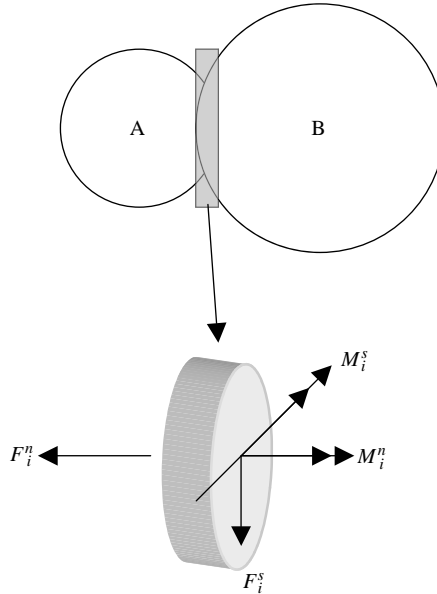


**Figure 1.**  
Force and moment  
components of a parallel  
bond cohesive interaction

$$F_{(i)} + F_{(i)}^d = M_{(i)}A_{(i)}; \quad (3)$$

where  $F_{(i)}$ ,  $M_{(i)}$ , and  $A_{(i)}$  are the generalized force, mass and acceleration components, respectively, and  $F_{(i)}^d$  is the damping force:

$$F_{(i)}^d = -\alpha|F_{(i)}|sign(V_{(i)});$$

$$sign(y) = \begin{cases} +1, & \text{if } y > 0; \\ -1, & \text{if } y < 0; \\ 0, & \text{if } y = 0 \end{cases} \quad (4)$$

where  $\alpha$  is the numerical damping (the detailed description can be found in the PFC<sup>3D</sup> manual). After some pre-process numerical simulation tests, the numerical damping factor is set to 0.15 and 0.05 for the concrete element and the reinforcement element, respectively.

### 2.1 Local parameters identification process

The goal is to model a structure, in which some of the macroscopic material properties (Young's modulus, Poisson's ratio, tensile and compressive strengths) are known. The structure's geometry is discretized with a collection of DE. To each of these elements a set of local parameters is assigned so that the macroscopic behavior of this collection is representative of the real material. This procedure is fully described in Hentz *et al.* (2003) and is based on the simulation of quasi-static uniaxial compression/traction tests.

A tri-axial test model is pre-developed in PFC<sup>3D</sup> and for a standard-sized specimen:

- (1) a compact, polydisperse DE collection is generated;
- (2) an elastic compression test is run with local elastic parameters given by the "macro-micro" relations; and
- (3) compressive and tensile rupture axial tests are simulated to deduce the remaining local parameters.

By performing these tests, the local parameters  $kn$ ,  $ks$ ,  $pb\_kn$ ,  $pb\_ks$ ,  $pb\_nstrength$ ,  $pb\_sstrength$  are set such that the global mechanical properties of the collection of DE are, as close as possible, to those of a concrete with a 35 GPa Young's modulus and a 30 MPa compressive strength.

Then, when simulating the first impact test, some readjustments were needed to fit the experimental data set. This readjustment procedure was performed only once (in the D22 impact test chosen as the reference test case) and the exact same set of parameters was used in all subsequent impact test cases to demonstrate the predicting capability of the method. The input numerical data are given in Tables I and II.

### 2.2 Introducing reinforcement

As in work by other authors (Meguro and Hakuno, 1989; Masuya *et al.*, 1994), reinforcement bars are represented as lines of elements placed next to one another, which have the same diameter as the diameter of the rebar. In the CEA-EDF test data, there are four reinforcement layers placed at equal-distances in the concrete target slab.

The same geometrical configuration is used in the numerical model and parallel bonds are used between the rebar elements.

In terms of the local behavior of the reinforcement elements, a simplified model is used here: instead of the elastic-plastic behavior observed in steel rebars only an elastic-brittle behavior is considered, because plasticity is not defined in PFC<sup>3D</sup>. To overcome this limitation the rupture threshold of the elastic-brittle behavior law has been artificially increased.

### 2.3 Discrete element modeling

2.3.1 *The concrete target slab.* The reinforcement pattern is shown in Figure 2. The isotropic and polydisperse packing of “concrete” elements is obtained through a disorder technique available in PFC<sup>3D</sup>, around the reinforcement lines. A parallel bond was applied between the concrete elements.

The following procedure was used to set up the model:

- (1) Generate six walls (a box) which correspond to the edges of the target, i.e.  $1.46 \times 1.46 \times 0.208$  m (as to tests D35 and D37, the box size should be replaced by  $1.46 \times 1.46 \times 0.416$  m).
- (2) Generate the reinforcement elements and set their transition and rotation ability to zero.
- (3) Generate the concrete elements in an arbitrary way. During this step, all movement between concrete elements is allowed, and the algorithm stops when equilibrium is reached.
- (4) Set the parallel bonds between all concrete elements, then delete the front wall and the back wall which correspond to the impact direction.
- (5) Release the reinforcement elements.

This procedure is followed to avoid obtaining an undesirable residual contact force between two elements during the DE generation. The total number of DE in the concrete slab is 19,403, with a radius distribution size between 0.005 and 0.02 m.

**Table I.**  
Parameters used in the model for the concrete (nomenclature of PFC<sup>3D</sup> is used)

Parallel-bond normal stiffness Pb_kn (Pa/m)	$70 \times 10^9$
Parallel-bond shear stiffness Pb_ks (Pa/m)	$14 \times 10^9$
Parallel-bond maximum normal stress Pb_nstrength (Mpa)	230
Parallel-bond maximum shear stress Pb_sstrength (Mpa)	23
Numerical damping $\alpha$	0.05
Friction coefficient $\mu$	0.3
Density $\rho_c$ (kg/m <sup>3</sup> )	2,500

**Table II.**  
Parameters used in the model for the steel reinforcement (nomenclature of PFC<sup>3D</sup> is used)

Parallel-bond normal stiffness Pb_kn (N/m)	$21,000 \times 10^9$
Parallel-bond shear stiffness Pb_ks (N/m)	$5,250 \times 10^9$
Parallel-bond maximum normal stress Pb_nstrength (Mpa)	3,500
Parallel-bond maximum shear stress Pb_sstrength (Mpa)	1,250
Numerical damping $\alpha$	0.15
Friction coefficient $\mu$	0.3
Density $\rho_c$ (kg/m <sup>3</sup> )	28,000

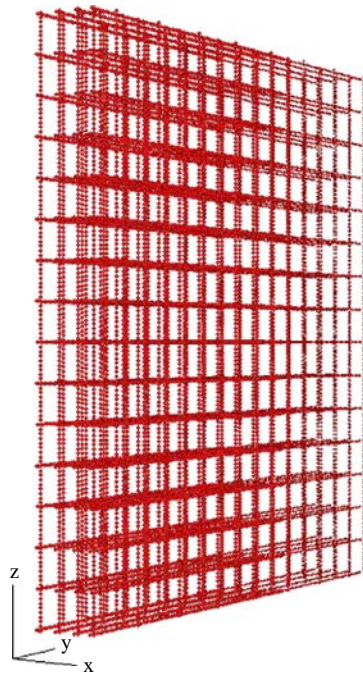


**Figure 2.**  
The four reinforcement  
layers of the concrete slab,  
represented by a set of  
17,408 DE

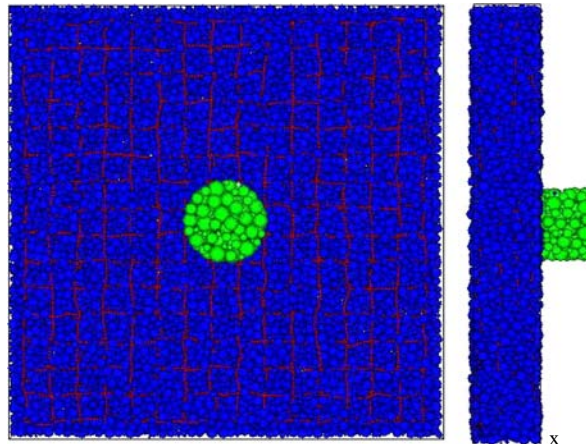
2.3.2 *The block.* Its geometry is as close as possible to the experimental one. The “clump” command has been used to simulate the missile, thus all the elements located in this clump can move together as well, so the missile was treated as a rigid body. The diameter and the weight of the missile are kept the same as in the CEA-EDF test, and the local parameters are identical those of the slab.

2.3.3 *Computation conditions.* Prior to any computation, gravity is applied on the slab until equilibrium is reached. The block is initially placed just above the slab surface, with the initial velocity corresponding to its impact velocity. The impact configuration (position and orientation) has been set as close as possible to the observed experimental configuration. On each side, a layer of 10 cm is fixed during the calculation. This gives a boundary condition. The block is subjected to gravity as well (Figure 3).

### 3. Modelling of impact tests

#### 3.1 CEA-EDF tests

The experimental shots were performed by the French Atomic Energy Agency (CEA) and the French Electrical Power Company (EDF) on reinforced concrete slabs, the thickness of which was chosen to represent, in a realistic way, the thickness of the wall of a reactor containment (Berriaud *et al.*, 1978). Seven tests have been chosen among all the CEA-EDF tests for the numerical simulation. The properties of the concrete material and the geometric shape of the missile (flat nose) were kept constant. The effects of parameters such as the missile velocity (25-450 m/s), its mass (20-300 kg), the ratio of the missile diameter to the thickness of the slab (0.24-2.9) and characteristics of the steel reinforcement were studied (Tables III and IV).



**Note:** Because of the coarse size of the concrete Discrete Elements, the first reinforcement layer is visible

**Figure 3.**  
On left, front view of the initial configuration of the impact process, on the right, the side view

**Table III.**  
CEA-EDF tests –  
concrete slabs

Shot	Concrete slab		Observation	
	Thickness (m)	Strength (Mpa)	Perforation (by PFC <sup>3D</sup> )	Penetration (m) (by equation (5))
D22	0.208	41.5	Yes	X
D24	0.208	38	No	0.05
D30	0.208	43.5	Yes	X
D27	0.208	44	Yes	X
D28	0.208	43.5	No	0.14
D35	0.416	38.5	No	0.285
D37	0.416	50	Yes	X

**Table IV.**  
CEA-EDF tests –  
missiles

Shot	Mass (kg)	Diameter (m)	Velocity (m/s)	Momentum (kgms <sup>-1</sup> )	Kinetic energy (kgm <sup>2</sup> s <sup>-2</sup> )
D22	34	0.278	151	$5.13 \times 10^3$	$3.88 \times 10^5$
D24	34	0.278	102	$3.47 \times 10^3$	$1.77 \times 10^5$
D30	34.5	0.278	186	$6.42 \times 10^3$	$5.97 \times 10^5$
D27	51.6	0.3	129	$6.66 \times 10^3$	$4.29 \times 10^5$
D28	32.8	0.3	153	$5.02 \times 10^3$	$3.84 \times 10^5$
D35	31	0.3	445	$1.38 \times 10^4$	$3.07 \times 10^6$
D37	303	0.1	49	$1.48 \times 10^4$	$3.64 \times 10^5$

### 3.2 Numerical results

The results of the tests involving a  $1.46 \times 1.46$  m concrete slab with a 0.208 m thickness reinforced by four different steel layers, impacted by a 34 kg non-deformable flat nose missile with a diameter of 0.278 m at velocities of 102, 151 and 186 m/s

were selected to be compared with the numerical model (tests D22, D24, D30). These velocities led to scabbing, penetration and perforation of the slab, respectively.

Gravity is applied to the slab until equilibrium is reached prior to any computation. The block is initially placed just beside the slab surface, with the initial velocity corresponding to its impact velocity. The impact configuration (position and orientation) has been set as close as possible to the observed experimental configuration (Figure 3).

The first results shown were obtained with the simulation of three tests with different impact velocities (102, 151 and 186 m/s, see Figure 4). The other parameters are the same for all three tests. The model can describe the different observed configurations such as, perforation, scabbing and penetration.

As soon as the damping factor is set for one of these tests, the model is capable of predicting the trajectory of the missile for the other two cases. Thus, when fixing the damping parameter for the test D22 (151 m/s), which induces penetration and scabbing processes, the model was able to reproduce the slight penetration for the 102 m/s impact velocity and the perforation process for the 186 m/s impact velocity (Figure 5).

The penetration depth was also calculated after numerical simulation for tests involving a simple penetration (no perforation had occurred; test D22, D28, D35), because these penetration test data are difficult to obtain, our numerical penetration results have been compared with the penetration prediction formula proposed by Li and Tong (2003), which has been deemed reliable in recent years:

$$\frac{X}{D} = \sqrt{\frac{(1 + k\pi/4N)4k}{(1 + I_d/N_d)\pi}} I_d, \quad \text{for } \frac{X}{D} \leq k \quad (5a)$$

$$\frac{X}{D} = \frac{2}{\pi} N_d \ln \left[ \frac{1 + (I_d/N_d)}{1 + (k\pi/4N_d)} \right] + k \quad \text{for } \frac{X}{D} > k \quad (5b)$$

where  $X$  is the penetration depth,  $D$  is the diameter of the missile,  $k$  is the dimensionless penetration depth, as a flat nose missile is used here,  $k$  is equal to 0.707, and two dimensionless numbers: the impact function  $I_d$  and the geometry function  $N_d$  which are defined as  $I_d = (Mv^2/D^3f_c)/82.6f_c^{-0.544}$ ,  $N_d = M/\rho_c D^3$  for a flat nose missile, where  $M$  is the mass of the missile,  $\rho_c$  is the density of a concrete target,  $v$  is the impact velocity and  $f_c$  is the compressive stress of a concrete target.

Li, Q.M. has also proposed a prediction formula for a small penetration depth, i.e. when  $X/D < 0.5$  the following equation should be used:

$$\frac{X_{test}}{D} = 1.628 \left( \frac{X_{anal}}{D} \right)^{2.789} \quad (5c)$$

The numerical results show a good agreement with equation (5) (where equation (5c) was used for test D24, see Table III). This is true up to test D35 which involves a thicker target (0.416 m). This could be due to the lack of plasticity in the reinforcement as well as the fact that ductility is not imposed in the concrete used in the numerical model. All in all the difference between the numerical results and the prediction formula for test D35 is about 20 percent.

After having identified the local parameters as explained previously and calibrated the damping parameter with the 151 m/s impact velocity test, some other tests were

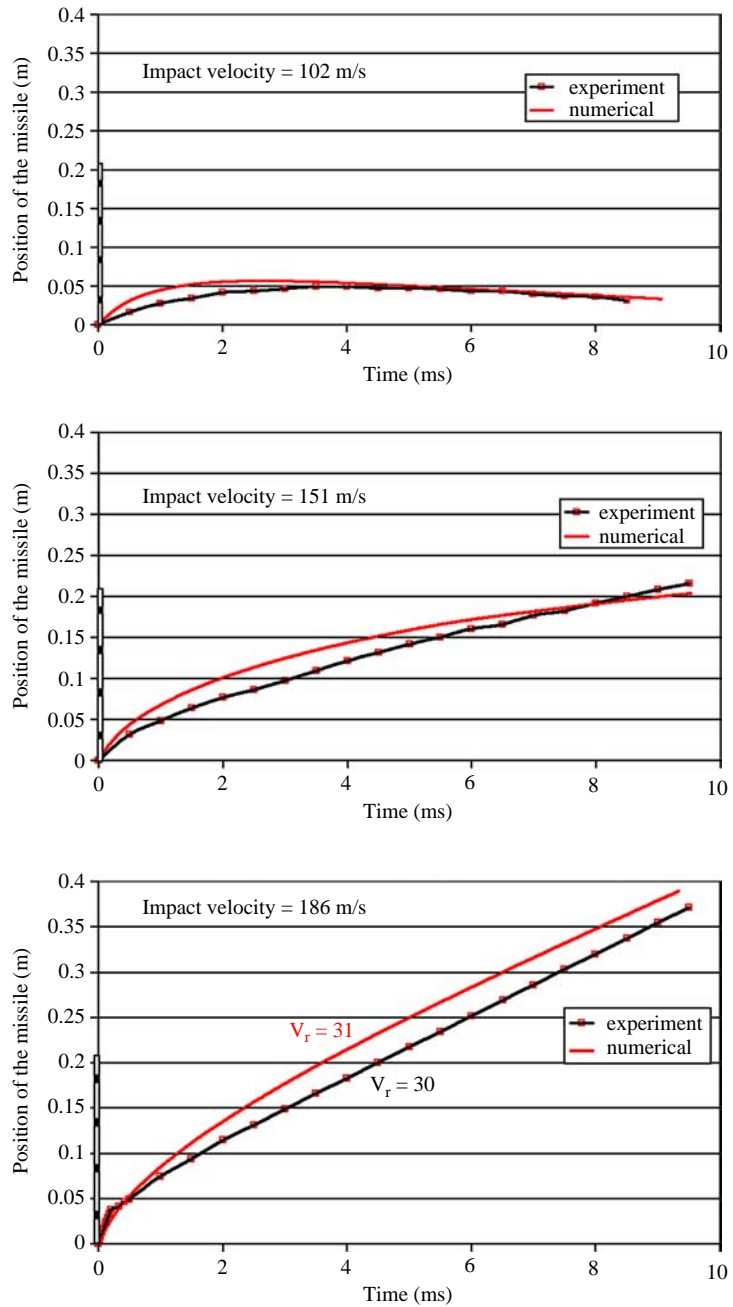


**Figure 4.**  
Comparisons between  
simulations and  
experiments for the three  
impact velocities: 102, 151  
and 186 m/s

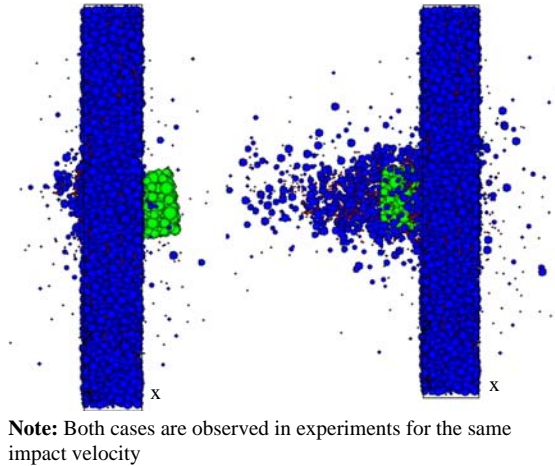


**Figure 5.** On the left, penetration case for the 102 m/s impact velocity (snap at 8.405 ms); on the right, perforation of the slab for the 186 m/s impact velocity (snap at 9.3 ms)

studied in order to analyze the influence of reinforcement and other parameters of the empirical formulae.

### 3.3 Influence of reinforcement ratio

The influence of the reinforcement ratio was analyzed and compared with an empirical formula derived from Berriaud *et al.*, 1978 and modified by the UK Atomic Energy Authority (Fullard *et al.*, 1991):

$$v_p = 1.3\rho_c^{1/6}f_c^{1/2} \left( \frac{Dd_p^2}{M} \right)^{2/3} (r + 0.3)^{0.5} \quad (6)$$

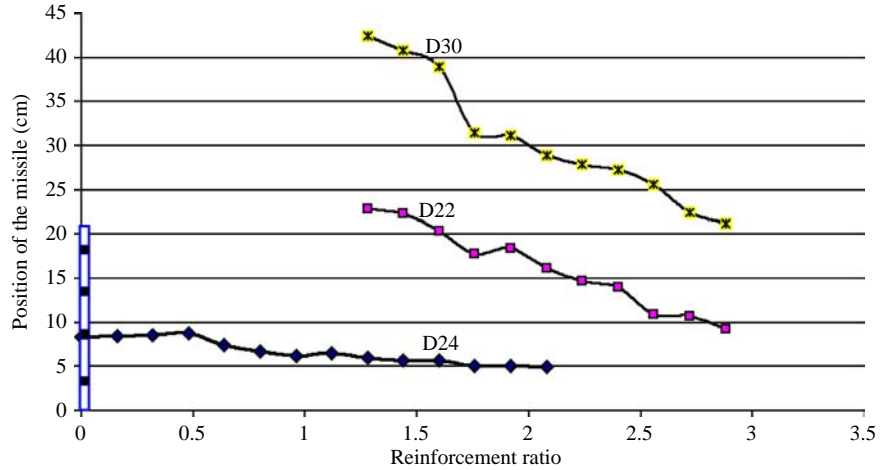
in which SI units are required.  $v_p$  (m/s) is the ballistic limit,  $\rho_c$  is the density of the concrete,  $f_c$  is the compressive strength of concrete,  $D$  is the missile diameter (flat nose),  $d_p$  is the slab thickness,  $M$  is the missile mass and  $r$  is the reinforcement ratio.

To change the reinforcement ratio in the numerical simulation instead of changing the diameter of an element, the yield stress of the parallel bond of all reinforcement elements has been increased (`pb_nstrength`, `pb_sstrength`). Thus, the effect of increasing the resistance of rebars is equivalent to increase the reinforcement ratio. The advantage of this procedure is that we can avoid a complicated element generating step as described in Section 2.3.

Equation (5) gives the correct prediction of perforation for tests D22 and D30. Figure 6 shows the influence of the reinforcement ratio on the penetration of the missile. There is no influence of the reinforcement ratio on the penetration depth since the initial velocity of the missile is much lower than the ballistic limit velocity. Also note that equation (5) predicts a perforation for a 102 m/s impact test and for a reinforcement ratio lower than 0.35 percent which is in opposition to the simulation results.

Tests D22 and D28 were also analyzed since they differ slightly but the perforation occurred only for test D22. Equation (5) predicts that there is no penetration in either

**Figure 6.**  
Influence of reinforcement ratio on missile position for tests D24 (102 m/s), D22 (151 m/s) and D30 (186 m/s)

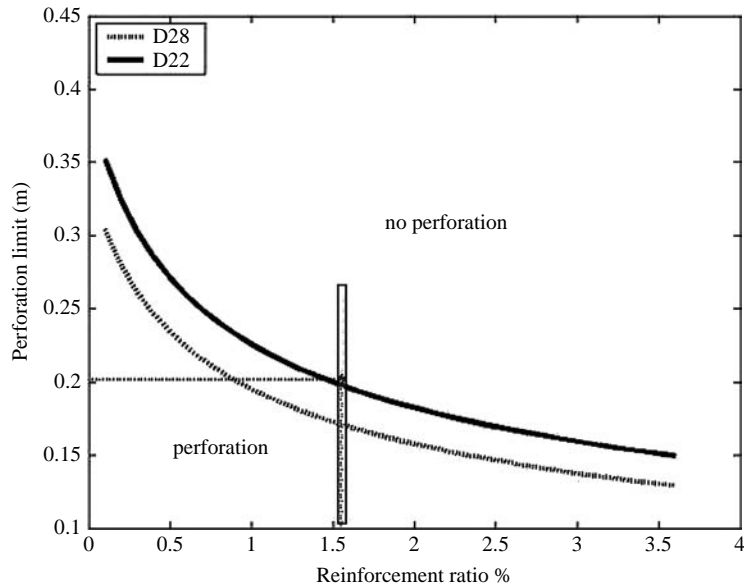


**Note:** Numerical

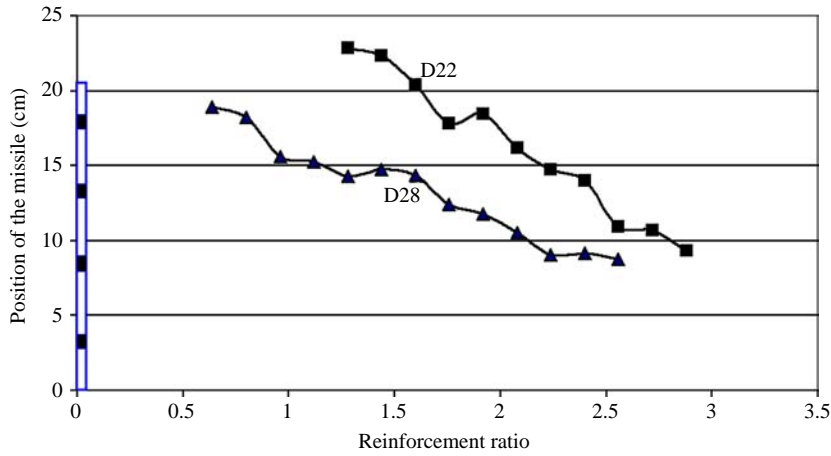
test (Figures 7 and 8) while the numerical simulation on the other hand correctly predicted the perforation.

Figure 9 shows the images captured after impact. The impact time duration was the same for all simulations. The penetration degrees for the different reinforcement ratios are easily distinguishable.

**Figure 7.**  
Influence of reinforcement ratio on missile position for tests D22 and D28



**Notes:** According to equation (5). Reproduced from the only available original



Note: Numerical

**Figure 8.** Influence of reinforcement ratio on missile position for tests D22 and D28

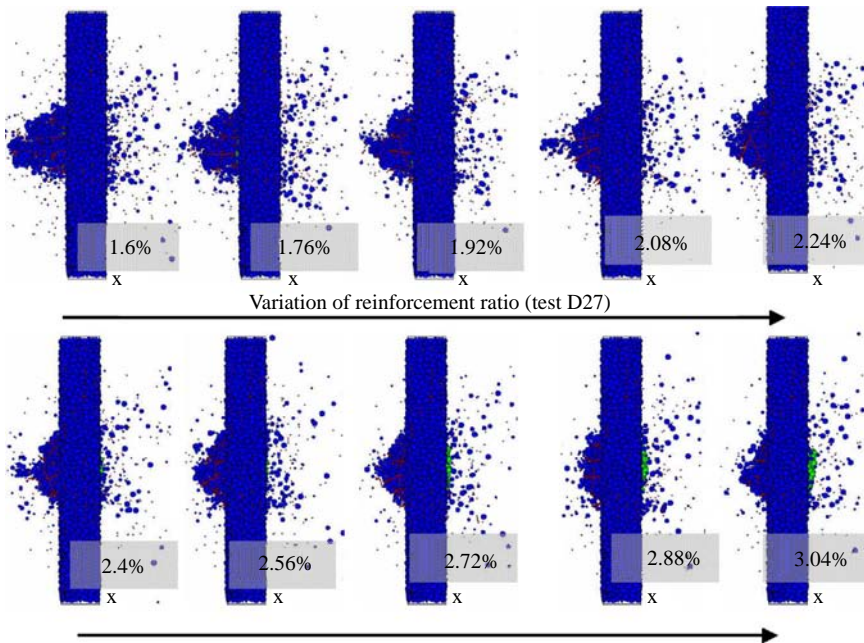


**Figure 9.** Influence of reinforcement ratio on the missile final position for test D27 (151 m/s), the perforation occurs for a reinforcement ratio < 2.24 percent

The concrete and the reinforcement elements were bonded together with parallel bonds (PFC<sup>3D</sup> code, 2003). In order to analyze the damage between the DE after impact, the percentage of broken bonds given by the numerical modeling has been calculated and shown in Figure 10. Considering that the target's surrounding is less damaged, we can concentrate on the impact zone which was considered as a square area around the

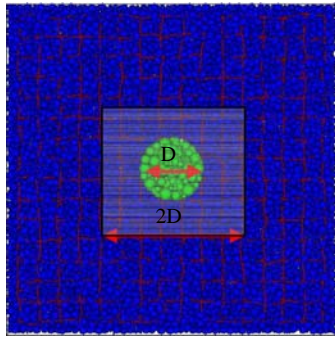
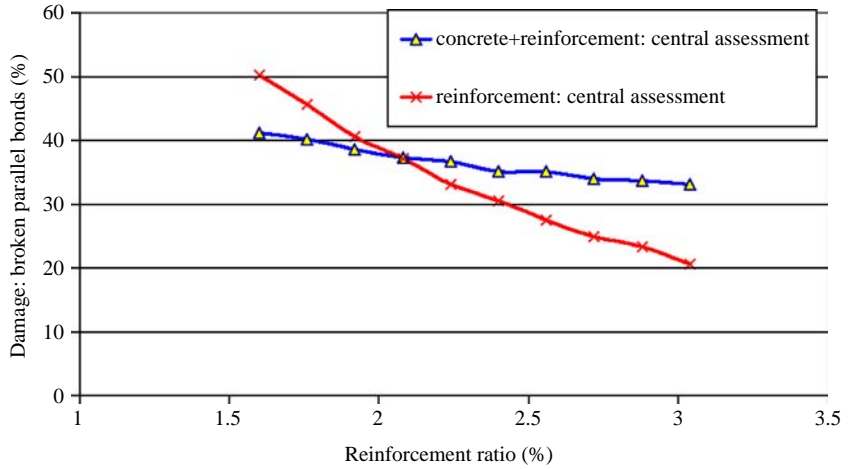


**Figure 10.**  
Influence of reinforcement ratio on percentage of broken bonds for test D27, in global assessment and central assessment

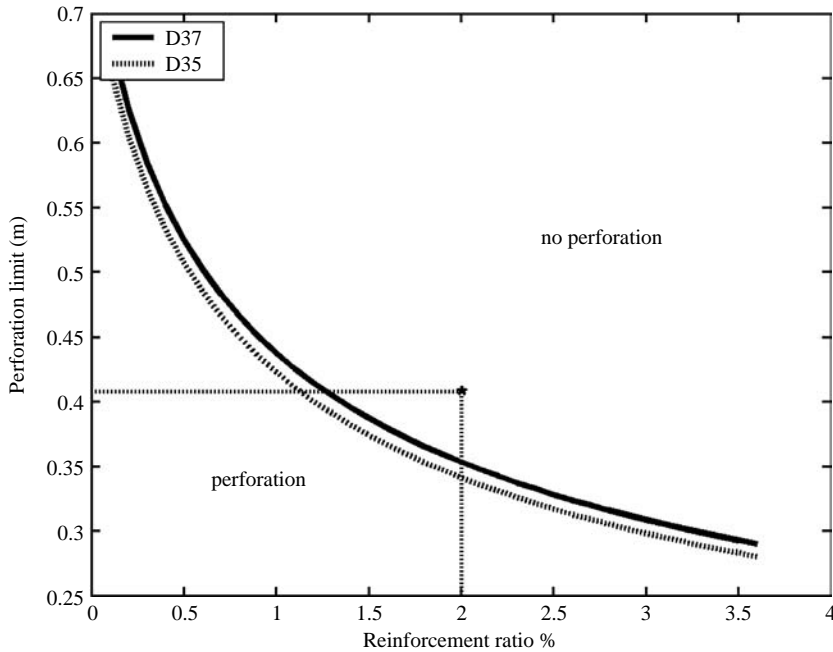
impact point (as shown in Figure 10). Serious damage was observed: the broken bonds of the rebars in this zone can vary considerably from 50 to 20 percent. Thus, for test D27, if the reinforcement ratio is increased to a certain percentage, the target can be well protected from missile penetration.

In test D35, one may observe that the final position of the missile can be separated into two parts depending on the reinforcement ratio. While the reinforcement ratio is less than 2 percent, the final position of the missile will be dominated seriously by the reinforcement, while the other part will not. This observation agrees with the empirical formulae, that is to say, the reinforcement will play an important role when the missile attempts to perforate the target. On the other hand, when the missile can easily penetrate the target, the influence of reinforcement can be ignored. This is why in recent empirical perforation formulae, the reinforcement is often considered within the ballistic limit.

Prior to the current work, there was little information about the effect of the reinforcement ratio in a concrete target during a missile impact. The numerical approach makes it possible to study this parameter. According to our numerical simulations, the reinforcement could play an important role when the target tends to be perforated.

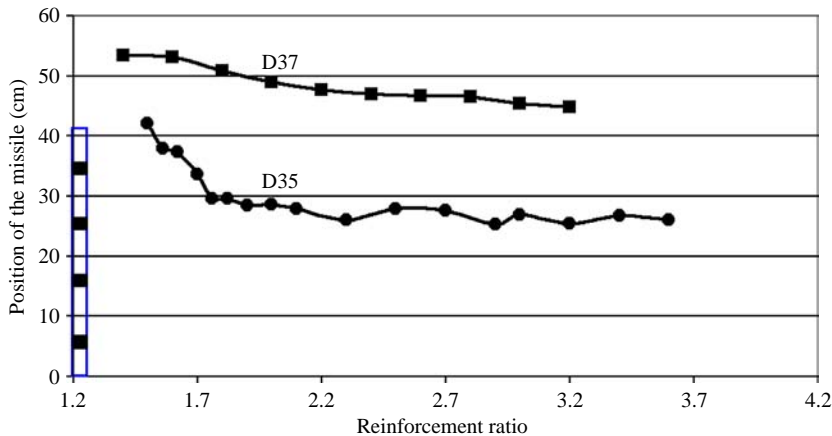
3.4 Kinetic energy and momentum

Tests D35 and D37 are close in terms of momentum but test D35 corresponds to a much higher kinetic energy. The DE model could correctly predict the perforation and penetration phenomena for both tests whereas equation (5) could not. The numerical results and the result predicted by equation (5) are shown in Figures 11 and 12. As shown in Figure 11 the two tests are very close. This means that considering two



Note: According to equation (5)

Figure 11. Influence of reinforcement ratio on missile position for tests D35 and D37



Note: Numerical

Figure 12. Influence of reinforcement ratio on missile position for tests D35 and D37

missiles, one with a low weight and high velocity (D35), and the other with a high weight and low velocity (D37), the two tests should have similar perforation behavior. According to experimental results, only D37 is perforated which is well reproduced in the numerical model (Figure 12). Some phenomena were noted during the numerical simulation: the impact energy of test D35, which involves a significant diameter (0.3 m) was dissipated quickly by the friction between the missile and concrete elements resulting in a sharp decrease of the impact velocity. As to test D37, which involves a small diameter, it is easier for the missile to perforate the target. When the missile is first launched, scabbing occurs, then if the missile has a high enough remaining velocity the complete perforation of the target takes place. Therefore, momentum and kinetic energy are not sufficient parameters to predict the perforation of concrete slabs.

#### 4. Conclusion

The main specificities of the 3D DE approach are the following: the modeling scale is higher than the heterogeneity scale, so the model may be used to simulate real structures, which means that the DEM is mainly used here for its ability to treat discontinuities; the interaction laws introduced are then very simple and are close to macroscopic laws; finally, an identification process based on quasi-static tests is used, so the quasi-static behavior of concrete is reproduced. This identification process is the key point, to allow a complete predictive computation.

In this work, the CEA-EDF impact tests were studied and simulated with this model, for different impact velocities, on a reinforced concrete slab at a real scale. Results were compared with experimental results: quantitatively results are very coherent with respect to experimental results. Moreover, using parametric studies, the numerical model has given interesting insights on the role of the reinforcement during the perforation process in a better way than the classical predictive empirical formulations. The numerical simulation results have shown that the reinforcement ratio has little influence on the penetration depth since the impact velocity is not close to the ballistic limit to perforate the target. On the other hand, the reinforcement ratio has a strong influence on the missile residual velocity and on damage in concrete in case of perforation.

#### References

- Berriaud, C., Sokolovsky, A., Gueraud, R., Dulac, J. and Labrot, R. (1978), "Local behavior of reinforced concrete walls under missile impact", *Nuclear Engineering and Design*, Vol. 45 No. 2, pp. 457-69.
- Camborde, F., Mariotti, F. and Donzé, F.V. (2000), "Numerical study of rock and concrete behavior by discrete element modelling", *Computers and Geotechnics*, Vol. 27 No. 4, pp. 225-47.
- Cundall, P.A. and Strack, O.D.L. (1979), "A discrete numerical model for granular assemblies", *Géotechnique*, Vol. 29 No. 1, pp. 47-65.
- Degen, P.P. (1980), "Perforation of reinforced concrete slabs by rigid missiles", *ASCE Journal of the Structural Division*, Vol. 106 No. 7, pp. 1623-42.
- Donzé, F.V. and Magnier, S-A. (1997), "Spherical discrete element code", Discrete Element Project Report No. 2, GEOTOP, Université du Québec à Montréal, Montreal.
- Fullard, K., Baum, M.R. and Barr, P. (1991), "The assessment of impact on nuclear power plant structures in the United Kingdom", *Nuclear Engineering and Design*, Vol. 130 No. 2, pp. 113-20.

- 
- Hentz, S., Daudeville, L. and Donzé, F.V. (2003), "Identification and validation of a discrete element model for concrete", *Journal of Engineering Mechanics*, Vol. 130 No. 6, pp. 709-19.
- Hughes, G. (1984), "Hard missile impact on reinforced concrete", *Nuclear Engineering and Design*, Vol. 77 No. 1, pp. 23-35.
- Iwashita, K. and Oda, M. (2000), "Micro-deformation mechanism of shear banding process based on modified distinct element method", *Powder Technology*, Vol. 109, pp. 192-205.
- Li, Q.M. and Tong, D.J. (2003), "Perforation thickness and ballistic limit of concrete target subjected to rigid projectile impact", *Journal of Engineering Mechanics*, Vol. 129 No. 9, pp. 1083-91.
- Li, Q.M., Reid, S.R., Wen, H.M. and Telford, A.R. (2006), "Local impact effects of hard missiles on concrete targets", *International Journal of Impact Engineering*, Vol. 32 Nos 1/4, pp. 224-84.
- Magnier, S.A. and Donzé, F.V. (1998), "Numerical simulations of impacts using a discrete element method", *Mechanics of Cohesive-frictional Materials*, Vol. 3 No. 3, pp. 257-76.
- Masuya, H., Kajikawa, Y. and Nakata, Y. (1994), "Application of the distinct element method to the analysis of the concrete members under impact", *Nuclear Engineering and Design*, Vol. 150 Nos 2/3, pp. 367-77.
- Meguro, K. and Hakuno, M. (1989), "Fracture analyses of concrete structures by the modified distinct element method", *Structural Engineering/Earthquake Engineering*, Vol. 6 No. 2, pp. 283-94.
- PFC<sup>3D</sup> code (2003), *PFC<sup>3D</sup> (Particle Flow Code in 3 Dimensions), Version 3.0*, Itasca Consulting Group Inc., Minneapolis, MN.
- Potapov, A.A., Hopkins, M.A. and Campbell, C.S. (1995), "A two-dimensional dynamic simulation of solid fracture part I: description of the model", *International Journal of Modern Physics*, Vol. 6 No. 3, pp. 371-98.
- Potyondy, D.O., Cundall, P.A. and Lee, C.A. (1996), "Modelling rock using bonded assemblies of circular particles, in rock mechanics tools and techniques", *Proceedings of the Second North American Rock Mechanics Symposium, Montréal, Canada*, June, pp. 1937-44.
- Riera, J.D. and Iturrioz, I. (1998), "Discrete elements model for evaluating impact and impulsive response of reinforced concrete plates and shells subjected to impulsive loading", *Nuclear Engineering and Design*, Vol. 179 No. 2, pp. 135-44.
- Williams, M.S. (1994), "Modeling of local impact effects on plain and reinforced concrete", *ACI Structural Journal*, Vol. 91 No. 2, pp. 178-87.

### Corresponding author

Wenjie Shiu can be contacted at: [wen-jie.shiu@hmg.inpg.fr](mailto:wen-jie.shiu@hmg.inpg.fr)